Hindawi
Journal of Control Science and Engineering
Volume 2020, Article ID 6502028, 9 pages
https://doi.org/10.1155/2020/6502028

Research Article

Coordinated Optimal Control of Secondary Cooling and Final Electromagnetic Stirring for Continuous Casting Billets

Dongsheng Wu,[1] Zhenping Ji,[1] Jian Yang,[2] Hongwei Gao,[1] Jiahui Yu,[1,3] and Zhaojie Ju[3]

[1]*School of Automation and Electrical Engineering, Shenyang Ligong University, Shenyang 110159, China*
[2]*School of Information Science and Engineering, Northeastern University, Shenyang 110819, China*
[3]*School of Computing, University of Portsmouth, Portsmouth, PO1 3HE, UK*

Correspondence should be addressed to Zhenping Ji; jizhenping@163.com and Hongwei Gao; 30963915@qq.com

Received 7 October 2019; Accepted 8 May 2020; Published 25 May 2020

Academic Editor: Sing Kiong Nguang

Secondary cooling and final electromagnetic stirring (F-EMS) are both key technologies for continuous casting. These parameters are usually optimized and controlled separately which caused internal quality fluctuations in unsteady conditions. In this paper, a coordinated optimal control strategy based on a multiobjective particle swarm optimization (MOPSO) algorithm is proposed for the parameter optimization of secondary cooling and F-EMS, which is solved based on multiobjective particle swarm optimization (MOPSO) algorithm. The solidification and heat transfer model are developed for the computation of billet temperature and the solidification, and the adaptive grid method is used to improve the diversity and robustness of optimal solutions. The secondary cooling water and F-EMS' stirring current are dynamically controlled based on the optimization results. The results of field trials showed that the maximum carbon segregation and other quality indexes of billets can be improved significantly.

1. Introduction

Continuous casting of steel is a process that molten steel is solidified into "semifinished" products, such as billets, blooms, and slabs, which are subsequently sent for rolling in the mills. At the beginning of continuous casting, as steel composition is qualified, molten steel is transported to the continuous caster with a ladle. From the ladle, molten steel is poured into a tundish and then into copper molds with a certain shape, which is cooled by high-speed water. In the mold, primary cooling occurs and makes a supporting solidified shell with molten steel inside. Then, the strand is continuously withdrawn through a series of secondary cooling zones (SCZs) where water cooling happens with sprays. When exit from the secondary cooling zones, the strand is cooling off by radiation in the air. And finally, it is cut into fix-length strips and transported to rolling mills for further processing. The process is schematically shown in Figure 1.

In the continuous casting process, electromagnetic stirring is commonly used to improve the billet quality, including mold electromagnetic stirring (M-EMS), secondary cooling electromagnetic stirring (S-EMS), and final electromagnetic stirring (F-EMS). Among them, F-EMS is supposed to be the key to improve the central quality of products, such as central segregation and porosity [1]. Otherwise, secondary cooling plays an important role in temperature distribution, greatly influencing the billet quality, such as internal cracks, segregation, and porosity.

However, secondary cooling and F-EMS are conventionally treated as two independent technologies without considering their interaction, and their parameters are generally optimized separately [2–4]. In the conventional model, secondary cooling water flows are determined by steel grade and size of billet and optimized as functions of casting speed for a specific caster. In the optimization, the corresponding constraint conditions include metallurgical criteria and serial control goals, and most of them are concerning about temperature distribution. Otherwise, the parameters including the installation position of F-EMS are determined according to the comprehensive situation of the

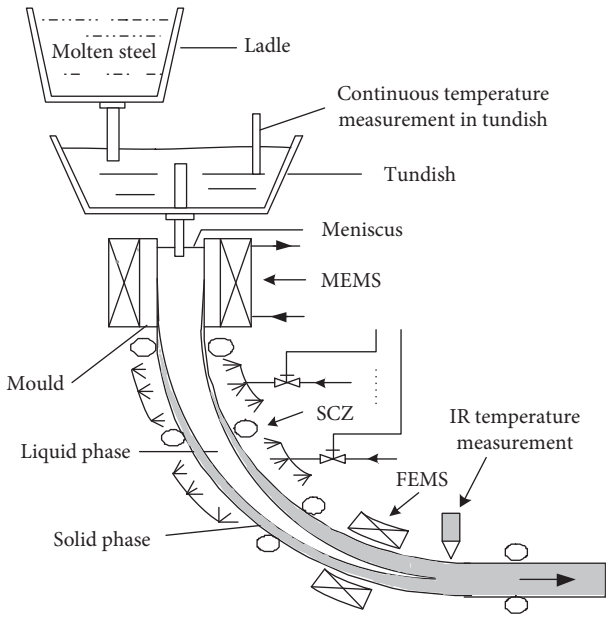

Figure 1: Diagram of billet continuous casting machine.

casting machine, which often remains unchanged in the production process. A billet caster often manufactures billets with different sizes and different steel grades, which results in the change of liquid core at the F-EMS position. Even for the same steel, the liquid core also changes due to factors such as production rhythm and molten steel temperature variety. According to the changing situation, if stirring parameters remain unchanged, obviously the F-EMS cannot play a proper role to keep the stability of solidification or even cause side effects. However, to keep the stability of the liquid core just by adjusting the secondary cooling water flows, that may lead to excessive temperature deviations from the target value and cause cracks and other quality problems [2]. Otherwise, if stirring parameters change according to the size area of the liquid core at F-EMS position without adjusting the water flows, as the liquid core is too big or too small, FEMS also cannot achieve its proper role. Therefore, the coordinated optimal control of secondary cooling and F-EMS is practically significant to improve the quality of casting billet.

In the coordinated optimal control problem, there are some difficulties including complex solution space and nonlinear and nondifferentiable objective functions due to the solidification process, as the steel solidification process belongs to the Stefan problem. To solve this multiobjective optimization problem (MOOP), conventional optimization methods are not suitable. In the past few years, swarm intelligence techniques are becoming increasingly popular for improving the process, including genetic algorithm [5, 6], particle swarm optimization (PSO) algorithms [7], and evolutionary multiobjective optimization algorithm [8, 9]. Among these techniques, PSO is most attractive for its high convergence speed and better exploration results. Normally, the MOOP is converted into a single objective optimization problem with classical weighted sum method by using a single pair of fixed weights and only one point on the Pareto frontier can be obtained, which is not suitable for the situation that if the optimal solutions lie on nonconvex or discontinuous regions of function space. Therefore, to obtain the global Pareto optimum, a well-spread and diverse Pareto solution frontier must be derived firstly, and it requires that the algorithms can be executed iteratively to ensure that any combination of weights is available. PSO is an intelligent evolutionary algorithm proposed by Eberhart and Kennedy [10], which is an effective metaheuristic for solving portfolio selection and then the successful applications motivated the researchers to apply it to multiobjective optimization problems [11, 12]. When developing multiobjective particle swarm optimization (MOPSO) algorithm, we will focus on the following three questions: (1) taking into account the diversity and ultimately convergence of Pareto fronts; (2) choosing the globally optimal solution (gBest) and local optimal solution (pBest) to guide the swarm particles to search for new solutions; and (3) try to be convergent and avoid falling into the local Pareto front.

In this paper, aiming at improving the production quality of continuous casting billets such as macrosegregation of high-carbon steels, a coordinated multiobjective optimization and control strategy is developed based on solidification and heat transfer model. The optimal solution and research results are applied to the dynamic control of the actual billet caster and good effects have been achieved.

2. Overview of the Optimal Control Strategy for Quality Control of Continuous Casting Billets

The framework for optimal control of secondary cooling and F-EMS is shown in Figure 2. It includes two parts: the coordinated optimization part and the dynamic control part. Above all, the heat transfer and solidification model serve as the basis of both parts, providing calculations of solidification states such as surface temperatures and radius of the liquid core. In the optimization part, a multiobjective particle swarm optimization (MOPSO) algorithm is adopted for coordinated optimization of secondary cooling and F-EMS. In the algorithm, the heat transfer and solidification model are used as the basis and the adaptive grid method is used to improve the diversity and robustness of solutions. In the dynamic control part, secondary cooling water flows and F-EMS stirring current are dynamically controlled based on the online model's calculations to avoid fluctuation of surface temperature and flow velocity in the solidification frontier, which benefits the quality stability.

3. Basis for Optimal Control Strategy—Heat Transfer and Solidification Model

The heat transfer process of continuous casting billets can be generally described by the heat transport equation. And the following assumptions are considered: (1) increasing heat conduction induced by the flow of nonsolid steel can be taken into account by an increased effective thermal conductivity; (2) the latent heat released during phase transformations can be considered in the equivalent specific heat;

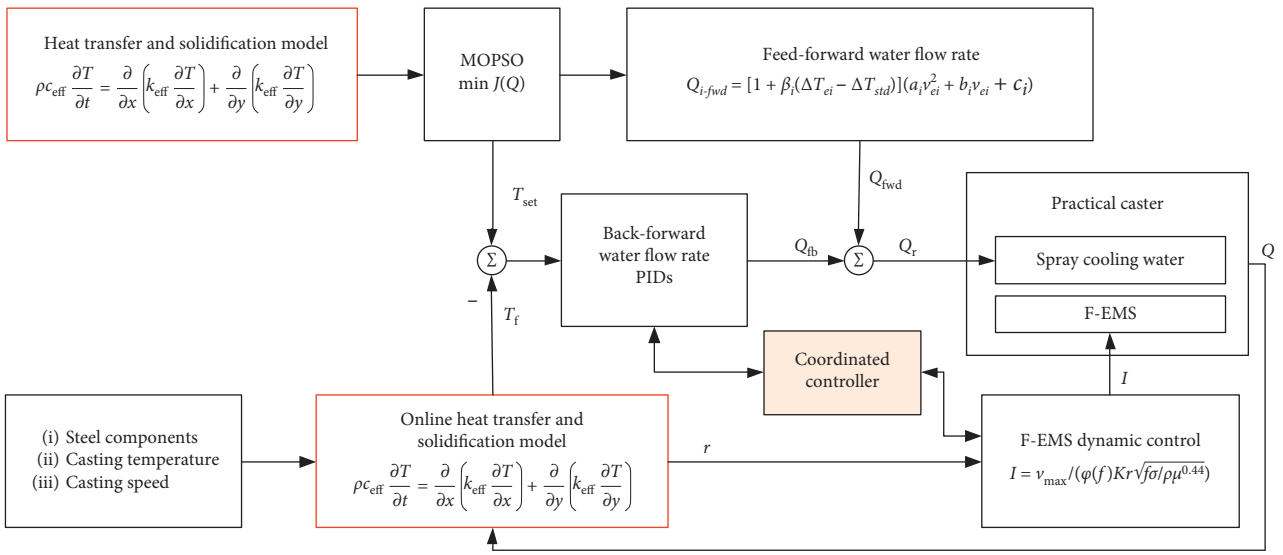

Figure 2: Framework of the optimal control strategy.

and (3) heat conduction in the casting direction can be ignored as it is quite small compared to the transverse cross-directions. The equation takes the following form in the follow-up coordinate system:

$$\rho c_{\text{eff}} \frac{\partial T}{\partial t} = \frac{\partial}{\partial x}\left(k_{\text{eff}} \frac{\partial T}{\partial x}\right) + \frac{\partial}{\partial y}\left(k_{\text{eff}} \frac{\partial T}{\partial y}\right), \quad (1)$$

where T is the billet temperature, t is the time, x and y are the coordinates, and ρ is the density of steel; $c_{\text{eff}} = \mathrm{d}H/\mathrm{d}T$, in which H is the enthalpy; $k_{\text{eff}} = f_s k_s + m\,(1 - f_s)\,k_l$, in which f_s is the solid fraction and k_s, k_l are separately the thermal conductivity of solid phase and liquid phase. The thermal properties including ρ, H, f_s, k_s, and k_l are assumed to be functions of T and of the steel compositions and can be calculated by a special algorithm based on pseudobinary phase diagram [13].

Considering the symmetry, only one-quarter of the billet slice (transverse cross-section) is selected as the calculation domain. Each slice starts at meniscus (assumed flat) and moves along the strand through the mold, secondary cooling zones, and then the air cooling zone.

The initial condition for each slice has been assumed to be the same as the casting temperature:

$$T = T_{\text{cast}}. \quad (2)$$

Moving down from the meniscus, each slice sequentially experiences the boundary conditions specified as follows.

In the mold, a type of decreasing heat flow due to air gap forming is considered [14]:

$$-k\frac{\partial T}{\partial n} = A - B\sqrt{t}, \quad (3)$$

where t is the experienced time of slice in the mold. In SCZ, water cooling and thermal radiation are considered:

$$-k\frac{\partial T}{\partial n} = h_i\left(T - T_w\right) + \varepsilon\sigma\left(T^4 - T_{air}^4\right), \quad (4)$$

where h_i is the heat transfer coefficient, ε is the emissivity, σ is the Stefan–Boltzmann constant, T_w is the cooling water temperature, and T_{air} is the air temperature. There can be two kinds of spays for different cooling zones. In the water spray cooling zones [15],

$$h = \frac{1570 w^{0.55}\left(1 - 0.0075 T_w\right)}{\alpha_i}, \quad (5)$$

where w is the water flow density (L/m^2/s). And in the air-mist spray cooling zones,

$$h = C_i w. \quad (6)$$

In equation (3), (5), and (6), A, B, α_i, and C_i are machine-dependent parameters. In the air cooling zone, thermal radiation is considered:

$$-k\frac{\partial T}{\partial n} = \varepsilon\sigma\left(T^4 - T_{\text{air}}^4\right). \quad (7)$$

In this study, the model is solved by FVM-ADI algorithm, discretized by the finite volume method, and solved by alternative direction implicit algorithm [14]. The temperatures and solidifications are computed as shown in Figure 3.

4. Coordinated Optimization of Secondary Cooling and the Final Electromagnetic Stirring Based on Multiobjective Particle Swarm Optimization Algorithm

4.1. Optimization Objective Functions. The billet quality depends on the behavior of the billet surface temperature and the flow of the solidification frontier. Undercooling of the strand can result in too long a liquid pool, and overcooling can lead to internal cracks. There must be a smooth transition of the surface temperature, with minimum reheating, as the steel passes from one cooling zone to another. The secondary cooling plays a major role in the

casting process because the intensity of the water sprays affects highly the solidification rate.

4.1.1. Billet Surface Temperature. The secondary cooling zone of the billet caster is divided into several sections. In each section, cooling water is dispersed to the billet surface to control the temperature filed. As target surface temperature is specified in each section, water flow rates Q_i ($i = 1, 2, ..., N$) of the secondary cooling zone should make billet surface temperatures match the target temperatures as closely as possible. So the cost function can be defined as follows:

$$f_1 = \frac{1}{2}\sum_{i=1}^{N}\left(T_i - T_i^*\right)^2, \tag{8}$$

where N denotes the number of sections and T_i and T_i^* are the calculated billet surface temperature and a target temperature of section i, respectively.

4.1.2. Liquid Core Size. There is also a requirement for liquid core size, namely, the radius of the liquid core at the center position of FEMS along the casting direction. To ensure the stability of liquid core size, the cost function f_2 is defined to make the radius of the liquid core as close as possible to the target value:

$$f_2 = \frac{1}{2}\left(r_{\text{liq}} - r_{\text{liq}}^*\right)^2. \tag{9}$$

4.1.3. Gradients of Surface Temperature. Besides, the gradients of the strand surface temperature along the casting directors should be controlled. Thus, the cooling rate C_{N} (°C/m) and reheating rate C_{p} (°C/m) are both considered. The cost function f_3 is defined as follows:

$$f_3 = \int_0^L \text{Max}\left(\frac{\partial T(z)}{\partial z} - C_p, 0\right)^2 dz + \int_0^L \text{Max}\left(C_N - \frac{\partial T(z)}{\partial z}, 0\right)^2 dz. \tag{10}$$

The optimization task is to minimize f_1, f_2, and f_3 according to possible cooling patterns, namely, water flow rate settings. As the three objective functions are conflicting, it is reasonable to handle this optimization problem by the multiobjective algorithm.

For different steel grades, the concerned quality problems to be solved are also different. So, the weight factors in the process of optimization should be changed accordingly.

4.2. Advanced Particle Swarm Optimization Algorithm. To solve the above optimization problem, an advanced particle swarm optimization algorithm is proposed. In the particle swarm optimization algorithm, it is supposed that the search space is d-dimensional and there are n particles in the swarm. Particle i is located at position $X_i = (x_{\text{i}1}, x_{\text{i}2}, \ldots, x_{id})$ and has velocity $V_i = (v_{i1}, v_{i2}, \ldots, v_{id})$. The update equations for velocity and position of the d-dimension and t generation are given as follows:

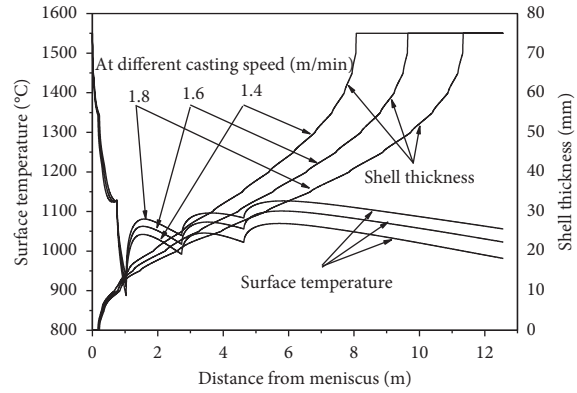

Figure 3: Temperature profile and solid shell thickness.

$$\begin{aligned} v_{\text{id}}(t+1) &= w_p * v_{\text{id}}(t) + c_1 r_1 * \left(p_{\text{id}} - x_{\text{id}}(t)\right) \\ &\quad + c_2 r_2\left(p_{\text{gd}} - x_{\text{id}}(t)\right), \\ x_{\text{id}}(t+1) &= x_{\text{id}}(t) + v_{\text{id}}(t+1), \end{aligned} \tag{11}$$

where $v_i(t)$ is the current velocity of i particle, $i = 1, ..., n$; n is the population size; the superscript i is the dimension of the particle; p_i is the best previous position of the i-th particle; p_g is the best previous position among all the particles in the swarm; $x_{\text{i}}(t)$ is the current position of the i-th particle. $i = 1, 2, \ldots, n$; w_p is nonnegative (inertia weight); c_1 and c_2 are the acceleration coefficients; r_1 and r_2 are the random numbers generated uniformly in the range [0, 1]; t is the current number of iterations.

By decreasing the inertia weight (w_p) from a relatively large value to a small value, the PSO tends to have better global search ability at the beginning and better local search ability near the end [3]. So, the inertia weight is set according to the following linear expression:

$$w_p = w_{\max} - N_{iter}\frac{w_{\max} - w_{\min}}{N_{\max}}, \tag{12}$$

where $N_{\max}$ is the maximum number of iterations and N_{iter} is the current number of iterations. Equation (14) restricts the value w to the range $w_{\max}$, $w_{\min}$. In this study, the maximum and minimum values of the inertia weights are set as 0.9 and 0.4, respectively.

To avoid the premature problem, mutation operation is adopted when the velocity of all particles is less than the limit value. The update functions are as follows [8]:

$$\begin{aligned} v_{\text{m}} &= 2(r_3 - 1)\beta v_{\max}, \\ x_{\text{id}}(t+1) &= x_{\text{id}}(t) + v_{\text{m}}, \end{aligned} \tag{13}$$

where v_m is the mutation value, β is the mutation coefficient between 0 and 1 used to adjust mutation degree, r_3 is the random number between 0 and 1, and x_{id} is the d-th dimension selected by random of i-th particle.

4.3. Pareto Optimal Solutions Based on Adaptive Grid Method. To maintain diversity in the Pareto optimal (nondominated) solutions, a novel mechanism with an adaptive grid is

introduced into the multiobject optimization algorithm (AD-MOPSO).

For optimization problem with r objectives, borders of the grid are set to $2r$ and a grid can be split into several small hypercubes (HC). The specific number of divisions is determined by the evolutionary population size and number of objectives. Supposing each HC as r^i, $i = i_1, i_2, \ldots, i_r$ and $i_k \in 1 \ldots d$, d is a constant number of divisions for each dimension.

In Figure 4, it is supposed that $d = 6$ and then corresponding to the side of each r^i can be expressed as follows:

$$rub_{k,i} = \left[lb_k + \left(\frac{i_k}{d}\right)(ub_k - lb_k)\right]\omega_k, \tag{14}$$

$$rlb_{k,i} = \left[lb_k + \left(\frac{i_k - 1}{d}\right)(ub_k - lb_k)\right]\omega_k, \tag{15}$$

where ω_k is the width of each region in k-dimension, $\omega_k = range_k/d$, in which $range_k$ is the width of k-dimension, $\forall k \in 1 \ldots r$.

Grid is a cube under the three-dimensional space for the three-dimensional objective function. The number of particles within each cube is determined by requiring a selection of the border and population size.

Let nondominated solutions set at generation t was obtained as A_t. The region width $range_k$ of each dimension is set as follows:

$$\text{range}_{k,t} = \max\{z_k \mid z \in A_t\} - \min\{z_k \mid z \in A_t\}. \tag{16}$$

Adaptive grids in the grid boundaries are not fixed. According to the present and the previous generation distribution of the individual, each generation evolution adaptively adjusts the boundary. If the newly generated individuals are located outside the boundaries of the previous generation and nondominated, it will be added to the archive set. If the archive set is full, other individuals will be deleted to ensure the distribution of the particles in the search space.

4.4. Pareto Optimal Solutions Weighting Computation. After obtaining many solutions that are true Pareto optimal with uniform spread coverage, a simple procedure called pseudo-weight vector approach is employed, which facilitates final decision making. In this approach, a pseudo-weight vector is calculated for each obtained solution [11]. The equation is given as follows:

$$w_{ij} = \frac{f_i^{\max} - f_{ij}(x)}{f_i^{\max} - f_i^{\min}}, \tag{17}$$

where w_{ij} is the weight of the i-th objective function for the j-th solutions, $f_i^{\max}$ and $f_i^{\min}$ are the maximum and minimum values of each objective function i in the obtained set of solutions, M is a number of the objective functions, and $f_{ij}(x)$ is the i-th objective function of the j-th solutions. The numerator on the right side of the above equation ensures that the sum of all weight components for a solution is equal to one.

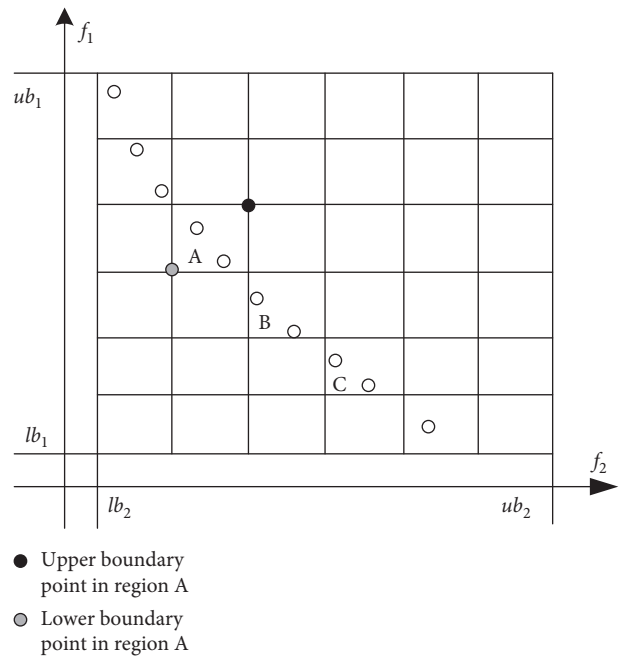

Figure 4: Grid and border.

Based on the optimization, the target value of the surface temperature of the second cooling zone and the liquid core radius of the final electromagnetic stirring position are obtained. The dynamic control of the secondary cooling and final electromagnetic stirring is realized by adjusting the secondary cooling water and control parameters of F-EMS.

5. Dynamic Control of Secondary Cooling and FEMS for Non-Steady State

5.1. Dynamic Control of Secondary Cooling for the Stability of Temperature. After optimization under different casting speeds, the secondary cooling water flows were determined. The water flows of secondary cooling zones were precisely controlled by a dynamic feed-forward strategy, described as follows:

$$Q_i = \left[1 + \beta_i\left(\Delta T_{ei} - \Delta T_{\text{std}}\right)\right]\left(a_i v_{ei}^2 + b_i v_{ei} + c_i\right), \tag{18}$$

where Q_i is the water flow of secondary cooling zone i, β_i is compensation coefficients of the superheat of cooling zone i, ΔT_{ei} is the effective superheat and ΔT_{std} is the standard superheat, v_{ei} is the effective casting speed [15, 16], and parameters a_i, b_i, and c_i are optimized spray cooling coefficients by MOPSO.

5.2. Dynamic Control of F-EMS' Stirring Current for the Stability of Flow Velocity of Liquid Steel. Stirring intensity of the solidification front can be expressed by the stirring velocity of molten steel. In the rotary stirring, the stirring velocity of the molten steel is calculated as follows [1]:

$$v = \sqrt{\frac{f\sigma}{\rho\mu^{0.44}}}, \tag{19}$$

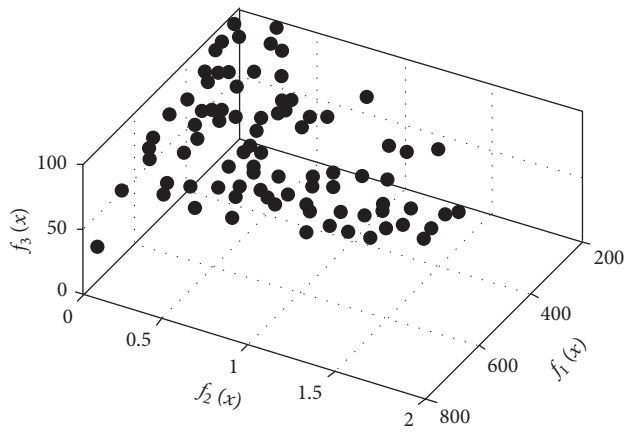

Figure 5: Pareto results of coordination optimization for secondary cooling and electromagnetic stirring (without adaptive grid trimming).

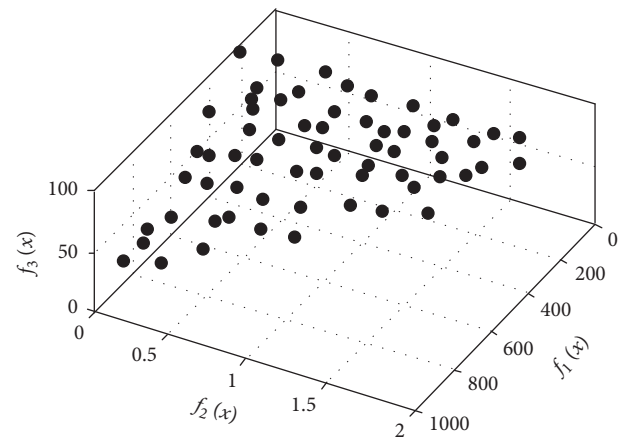

Figure 6: Nondominated solutions for three objective functions using MOPSO (with adaptive grid trimming).

where K is the constant related to a magnetic stirrer, B is the magnetic induction of billet center (Gs), f is the frequency of stirrer (Hz), r is the liquid core radius (two-phase region + liquid region, cm), σ is the electric conductivity of molten steel (s/cm), ρ is the molten steel density (g/cm3), and μ is the molten steel kinematics viscosity (CP, 1CP = 0.001 Pa·s).

The relationship between magnetic flux density (B) at the stirrer center and electric current (I) can be obtained from the measuring data and B was given as follows:

$$B = \varphi(f)I. \tag{20}$$

In the practical application, we first choose a suitable operating frequency of final electromagnetic stirrer and then determine the current value according to the corresponding liquid core radius and the target stirring velocity of the molten steel at the stirrer center. The current was calculated as follows:

$$I = \frac{B}{\varphi(f)} = \frac{v_{\max}}{\varphi(f)Kr\sqrt{f\sigma/\rho\mu^{0.44}}}. \tag{21}$$

6. Example Results

The above optimal control strategy for secondary cooling water and electromagnetic stirring has been applied in billet caster 1# of Sanming Iron and Steel Cooperation of China. Numerical experiments in MOOP of the casting process are performed for 65# steel with the billet size of 0.16 m × 0.16 m. The radius of the caster is 10 m. The caster has four cooling sections in the secondary cooling zone. The uppermost section is equipped with water sprays and the rest three are equipped with air-mist sprays. The length of the four sections is 0.37 m, 1.85 m, 2.20 m, and 2.32 m. The effective mold length is 0.90 m. FEMS is installed 7.70 m from the meniscus.

The prescribed target billet surface temperatures are adjusted for different casting speeds. For example, the prescribed target surface temperatures at the end of four zones are sequentially 924°C, 928°C, 948°C, and 962°C at a casting speed of 2 m/min. The initial parameters in PSO are set as follows: the initial population of MOPSO is set to 50, the number of generations is set to 100, $c_1 = 1.85$, $c_2 = 1.455$, $w = 1.0$, and the number of nondominated solutions to be found is set to 50.

The optimization problems are carried out for different casting speeds. The casting speeds used are changed from 1.6 m/min to 2.2 m/min with a step size of 0.1 m/min. Steady-state operation of the casting machine is assumed and optimization is performed in an off-line manner.

The optimization procedures were tested for both the solution quality and repeatability of results. The results of 50 nondominated solutions obtained using MOPSO after 100 iterations are shown in Figures 5 and 6. Several alternatives can be chosen at various satisfaction levels of the multiple objectives. Depending on steel grade and quality requirements and by analyzing the tradeoff between the multiple objectives, the researcher can make an appropriate decision.

To evaluate the performance of the proposed AD-MOPSO algorithm, these optimization results are compared to MOPSO without adaptive grid trimming. Due to the adaptive grid trimming and maintenance of the external archive set, the Pareto optimal solutions in Figure 6 have better distribution in the search space than those in Figure 5 and the Pareto distribution is more uniform. In the Cartesian coordinate system composed of three objective functions, the overall Pareto frontier distribution is in a plane shape. It can be seen from Figures 5 and 6 that AD-MOPSO gives a better distribution of true Pareto optimal solutions.

To reduce a large number of alternatives, the adaptive grid algorithm was used to filter the large set of nondominated solutions to a few representative solutions. Table 1 shows 30 representative Pareto optimal solutions for the three objective functions. Based on equation (21), the weights that can be given for each objective are shown in Table 1, which gives the objective values for each of the representative Pareto optimal solutions and their respective weight for each alternative. According to the different kinds of steel grade and quality requirements,

Table 1: Representative Pareto optimal solutions and weights at a casting speed of 2.0 m/min.

No.	f_1	w_1	f_2	w_2	f_3	w_3
1	222.48	0.77	1.29	0.23	87.54	0.00
2	244.99	0.95	1.82	0.00	84.38	0.05
3	256.15	0.57	0.66	0.39	82.96	0.04
4	257.60	0.61	0.87	0.35	82.83	0.05
5	267.88	0.50	0.35	0.45	82.37	0.04
6	289.64	0.78	1.65	0.09	77.97	0.13
7	308.16	0.59	1.11	0.28	75.53	0.13
8	311.44	0.56	0.99	0.31	75.38	0.12
9	312.89	0.43	0.20	0.47	75.55	0.09
10	313.15	0.48	0.55	0.41	75.34	0.11
11	350.03	0.63	1.46	0.17	70.87	0.21
12	378.43	0.54	1.25	0.24	68.17	0.22
13	382.12	0.38	0.24	0.47	67.92	0.16
14	383.79	0.45	0.82	0.36	67.87	0.19
15	389.87	0.39	0.45	0.43	67.25	0.17
16	409.79	0.52	1.36	0.21	64.77	0.27
17	452.92	0.37	0.77	0.37	60.80	0.26
18	466.44	0.31	0.38	0.45	59.99	0.23
19	472.87	0.47	1.48	0.16	58.90	0.37
20	491.03	0.27	0.11	0.49	57.15	0.24
21	510.30	0.37	1.25	0.25	55.66	0.38
22	523.17	0.33	1.05	0.31	54.51	0.36
23	571.70	0.25	0.80	0.38	50.71	0.37
24	576.44	0.21	0.41	0.46	51.52	0.32
25	579.58	0.19	0.07	0.52	50.84	0.29
26	593.57	0.18	0.80	0.32	27.59	0.50
27	596.50	0.16	0.38	0.40	27.85	0.44
28	630.98	0.13	0.32	0.41	26.92	0.45
29	744.71	0.03	0.38	0.43	22.13	0.53
30	781.35	0.00	0.05	0.51	24.06	0.49

decision-makers can choose a suitable solution for optimization control.

In actual casting process control, quality indexes for different steel grades are also different, so the weight of the objective functions is also different. Since the 65# steel has high carbon, high strength, hardness, and elasticity and low cold plastic deformation characteristics, it is easy to form center segregation and center shrinkage. F-EMS is usually used to improve billet quality and a higher weight of the cost function f_2 is desired.

In the optimization process, the weight coefficients choice depends on the steel grade and quality requirements. After analyzing the available alternatives, based on the analytic hierarchy process, the final decision can be made. The weights 0.25, 0.50, and 0.25 for f_1, f_2, and f_3 are selected which is closer to that set of weights of 20th solution from Table 1.

The corresponding fitting parameters of the secondary cooling control model with quadratic equation (26) are shown in Table 2.

The dynamic control of secondary cooling greatly reduced the fluctuation of midface temperature at the end of secondary cooling zones with the changing casting conditions.

The magnetic flux density of F-EMS is the maximum value at the frequency of around 8.5 Hz. While the frequency is greater than 10 Hz, the actual current will gradually deviate from (less than) the setting value and the magnetic flux density decreases, so the operating frequency is set at 9 Hz.

Table 2: Secondary cooling control parameters.

Parameters	Cooling zone			
	Zone 1	Zone 2	Zone 3	Zone 4
a_i	1.44	2.90	0.51	0.43
b_i	0.74	−3.00	−0.21	−0.18
c_i	0.90	2.90	0.75	0.64
β_i	0.00133	0.00113	0.00094	0.00071

Besides, equation (10) has also been applied to the dynamic control of the electric current of F-EMS. To control the stirring velocity of 0.15 m/s induced by F-EMS stirrer in the mushy zone, the F-EMS current has been set as a function of mushy zone radius at the installation position of F-EMS. Figure 7(a) presents the tuning of F-EMS current with the changing casting conditions. The radius of the mushy zone is influenced by the casting speed and superheat. As the radius of the mushy zone is increasing, the flow in the mushy zone accelerates; to keep the flow speed in the mushy zone stable, the F-EMS current is supposed to decrease accordingly. In this paper, the F-EMS current has been set to be proportional to the reciprocal of the mushy zone radius, as shown in Figure 7.

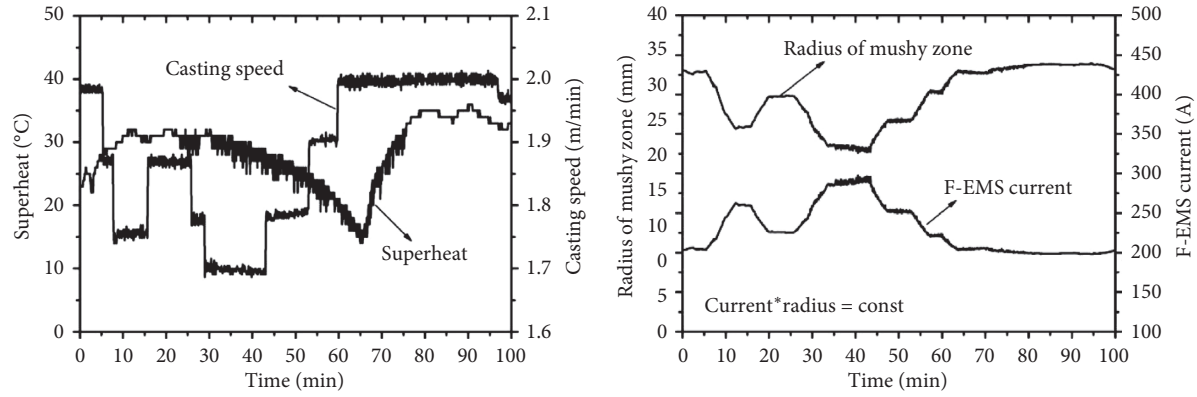

Figure 7: Dynamic control of F-EMS. (a) The casting conditions including pouring superheat and casting speed. (b) The radius of the mushy zone at F-EMS installation position and F-EMS current as functions of time.

Table 3: Distribution of billet internal defects.

Defect levels	Porosity (%)	Carbon segregation	Shrinkage cavity	Center crack
0	21.5	24.7%	75.0%	100%
0.5	63.2	60.3%	23.5%	0
1.0	13.8	15.0%	1.5%	0
>1.0	1.5	0	0	0

After the dynamic control strategy was applied in actual billet caster, the fluctuation of surface temperatures of billet in secondary cooling zones and the flow speed in the mushy zone were reduced. The defects of macrosegregation, porosity, and shrinkage cavity have been reduced significantly. Table 3 shows the distribution of billet internal defects of 180 sample macrographs.

7. Conclusions

In this paper, a coordinated optimal control strategy for secondary cooling and F-EMS has been proposed and applied to an actual caster. The optimized results are applied in the practical casting machine. Some conclusions could be drawn as follows.

An optimization method based on MOPSO for secondary cooling and FEMS of continuous casting is proposed and applied to the coordinated control of the billet continuous casting process. It integrates two independent control systems by coordinating weighting factors for various steel grades.

The improved Pareto multiobjective particle swarm optimization algorithm considers both convergence and diversity of Pareto optimal population. It also improved the robustness in yielding efficient Pareto frontiers.

A dynamic control model is developed and applied in the billet production process based on the coordinated control of secondary cooling water and stirring current of F-EMS. This ensures the stability of the surface temperature of the billets and the radius of the liquid core and reduces the fluctuation of surface temperature and flow velocity of liquid steel in the solidification frontier. Lots of industry trial results show that the carbon level is significantly improved. The maximum central segregation index is 1.06 and other internal quality problems are improved effectively.

Data Availability

The data named "billet caster 1# of Sanming Iron and Steel Cooperation of China" used to support the findings of this study are currently under embargo while the research findings are commercialized. Requests for data, 12 months after publication of this article, will be considered by the corresponding author.

Conflicts of Interest

The authors declare that there are no conflicts of interest regarding the publication of this paper.

Acknowledgments

The authors would like to acknowledge support from 4 projects: the National Natural Science Foundation of China (61273178 and 61703084), the Natural Science Foundation of Liaoning Province (20180550801), Liaoning Province Higher Education Innovative Talents Program Support Project (LR2019058), and the research support of Sanming Iron and Steel Cooperation of China.

References

[1] B. Mao, G. Zhang, and A. Li, *Theory and Technology of Electromagnetic Stirring for Continuous Casting*, Metallurgical Industry Press, Beijing, China, 2012.

[2] C. Xiao, J. Zhang, Y. Luo et al., "Control of macrosegregation behavior by applying final electromagnetic stirring for continuously cast high carbon steel billet," *Journal of Iron and Steel Research International*, vol. 20, no. 11, pp. 11–20, 2013.

[3] W. Su, W.-L. Wang, S. Luo, D.-B. Jiang, and M.-Y. Zhu, "Heat transfer and central segregation of continuously cast high

carbon steel billet," *Journal of Iron and Steel Research International*, vol. 21, no. 6, pp. 565–574, 2014.

[4] S. Luo, F.-Y. Piao, D.-B. Jiang, W.-L. Wang, and M.-Y. Zhu, "Numerical simulation and experimental study of F-EMS for continuously cast billet of high carbon steel," *Journal of Iron and Steel Research, International*, vol. 21, no. 1, pp. 51–55, 2014.

[5] N. Cheung and A. Garcia, "The use of a heuristic search technique for the optimization of the quality of steel billets produced by continuous casting," *Engineering Applications of Artificial Intelligence*, vol. 14, no. 2, pp. 229–238, 2001.

[6] C. A. Santos, J. A. Spim, and A. Garcia, "Mathematical modeling and optimization strategies (genetic algorithm and knowledge base) applied to the continuous casting of steel," *Engineering Applications of Artificial Intelligence*, vol. 16, no. 5-6, pp. 511–527, 2003.

[7] Z. P. Ji and Y. Y. Jiang, "Optimization of cooling parameters in casting processes based on adaptive evolutionary particle swarm algorithm," *Advanced Materials Research*, vol. 468-471, pp. 2399–2402, 2012.

[8] A. V. Lotov, G. K. Kamenev, V. E. Berezkin, and K. Miettinen, "Optimal control of cooling process in continuous casting of steel using a visualization-based multi-criteria approach," *Applied Mathematical Modelling*, vol. 29, no. 7, pp. 653–672, 2005.

[9] F. Bogdan, T. Tea, and L. Erkki, "Preliminary numerical experiments in multiobjective optimization of a metallurgical production process," *Informatica*, vol. 31, pp. 233–240, 2007.

[10] R. C. Eberhart and J. Kennedy, "A new optimizer using particle swarm theory," in *Proceedings of the 6th International Symposium on Micro Machine and Hunan Science*, pp. 39–43, IEEE Robotics and Automation Society, Nagoya, Japan. USA, October 1995.

[11] M. J. Reddy and D. Nagesh Kumar, "Multi-objective particle swarm optimization for generating optimal trade-offs in reservoir operation," *Hydrological Processes*, vol. 21, no. 21, pp. 2897–2909, 2007.

[12] I. Montalvo, J. Izquierdo, S. Schwarze, and R. Pérez-García, "Multi-objective particle swarm optimization applied to water distribution systems design: an approach with human interaction," *Mathematical and Computer Modelling*, vol. 52, no. 7-8, pp. 1219–1227, 2010.

[13] J. Yang, Z. Xie, J. Ning, W. H. Liu, and Z. P. Ji, "A framework for soft sensing of liquid pool length of continuous casting round blooms," *Metallurgical and Materials Transactions B*, vol. 45, 2014.

[14] J. Yang, Z. Xie, Z. Ji, and H. Meng, "Real-time heat transfer model based on variable non-uniform grid for dynamic control of continuous casting billets," *ISIJ International*, vol. 54, no. 2, pp. 328–335, 2014.

[15] Z. Ji, W. Liu, Z. Xie et al., "Coupling analysis of casting speed and tundish superheat controlling secondary cooling in continuous casting," *Iron Steel Vanadium Titanium*, vol. 28, no. 3, pp. 51–55, 2007.

[16] J. Yang, Z. Hu, and H. Meng, "Dynamic secondary cooling model for continuous casting based on temperature measurement," *Journal of Iron and Steel Research*, vol. 2, pp. 112–116, 2019.